Check for updates

Macromolecular Rapid Communications
www.mrc-journal.de

Dynamic Heterogeneity of Filler-Associated Interphases in Polymer Nanocomposites

*Horst Schneider, Matthias Roos, Yury Golitsyn, Kerstin Steiner, and Kay Saalwächter**

Dedicated to the memory of Aurelie Papon

Dynamically inhomogeneous polymer systems exhibit interphases with mobility gradients. These are believed to play key roles in the material's performance. A prominent example is particle-filled rubber, a special case of a crosslinked polymer nanocomposite, where favorable rubber-filler interactions may give rise to a nanoscale immobilized layer around the filler, including regions of intermediate mobility. Such intermediate domains may either form a separate shell-like layer or be a manifestation of dynamic heterogeneities, in which case the intermediately mobile material would be dispersed in the form of nanometer-sized subdomains. In this contribution, bidirectional proton NMR spin diffusion (SD) experiments applied to silica-filled acrylate rubber are combined with numerical simulations to provide microscopic insights into this question. While model calculations for different scenarios fit the given data similarly well for longer SD mixing time, the short-time data do support the presence of dynamic heterogeneities.

1. Introduction

Synthetic polymers are frequently reinforced with filler particles to achieve superior mechanical properties[1] and increased material longevity[2] of the resulting polymer nanocomposites (PNC) as compared to the pure polymeric material. Vital to these reinforcement effects is a network of partially aggregated filler particles[3] that are mechanically linked to each other through immobilized polymer segments.[4] Associated mechanisms have been explored and rationalized both theoretically[5–7] and experimentally,[8–14] showing that the strongest mechanic reinforcement of the compound material will be observed if the immobilized polymer layers overlap[7] so as to form "glassy bridges" between the filler particles.[6] The typical layer size of immobilized polymer segments around the filler is 1–2 nm,[10,15] where polymer immobilization is a consequence of strong attractive interactions of the polymer with, or chemical grafting to, the surface of the filler nanoparticle. A typical example of strong attractive interactions is bare silica particles, the free surface hydroxyl groups of which interact favorably with polymers capable of hydrogen bonding, such as poly(ethylene oxide) (PEO),[12,13,16,17] poly(dimethylsiloxane) (PDMS),[8,18] poly(2-vinyl pyridine) (P2VP),[10,19–21] and acrylate polymers.[9,22–25]

The effect of filler particles on polymer mobility is reminiscent of polymers under confinement, particularly surface restraints and associated effects on the glass transition temperature, T_g.[26] Empirically, the average T_g of polymer thin films has been found to scale with the layer thickness z,

$$T_g(z)/T_g^{bulk} = 1 \pm (\xi/z)^{\upsilon} \quad (1)$$

where υ is a parameter close to 1, and ξ is related to the amplitude and length scale of the T_g gradient relative to the glass transition temperature of the bulk material, T_g^{bulk} (see **Figure 1**a).[27,28] Chain immobilization upon absorption of polymer segments increases T_g over a distance of several nanometers (plus sign in Equation (1)).[29,30] The glass transition phenomenon is intrinsically coupled to the appearance of dynamic heterogeneity on the nanoscale, and the "percolation of free volume distribution" (PFVD) model[31–33] presupposes such heterogeneity to explain 3D glass transition phenomena as well as T_g gradients. In such a picture, a 1D T_g gradient along the interface normal arises as average over a laterally inhomogeneous distribution of dynamic heterogeneities of nm size within the interface region, the distribution of which changes with distance z (see Figure 1b).

For polymers at T_g + 10 K, the typical length scale of dynamical heterogeneities is ξ = 2–3 nm (order of 100 monomers)[34] and decreases to about 10 monomers at T_g + 80 K.[35] This suggests that the mobility gradient in particle-filled rubber might consist of local sub-domains with different mobility. Such a view was reinforced recently by experimental work by the Sokolov group, who found that the thickness of the

Prof. H. Schneider, Dr. M. Roos, Y. Golitsyn, Dr. K. Steiner,[+]
Prof. K. Saalwächter
Institut für Physik-NMR
Martin-Luther-Universität Halle-Wittenberg
Betty-Heimann-Str. 7, Halle 06120, Germany
E-mail: kay.saalwaechter@physik.uni-halle.de

The ORCID identification number(s) for the author(s) of this article can be found under https://doi.org/10.1002/marc.202100061.

[+]Present address: numares AG, Regensburg, Germany

© 2021 The Authors. Macromolecular Rapid Communications published by Wiley-VCH GmbH. This is an open access article under the terms of the Creative Commons Attribution-NonCommercial License, which permits use, distribution and reproduction in any medium, provided the original work is properly cited and is not used for commercial purposes.

DOI: 10.1002/marc.202100061

© 2021 The Authors. Macromolecular Rapid Communications published by Wiley-VCH GmbH

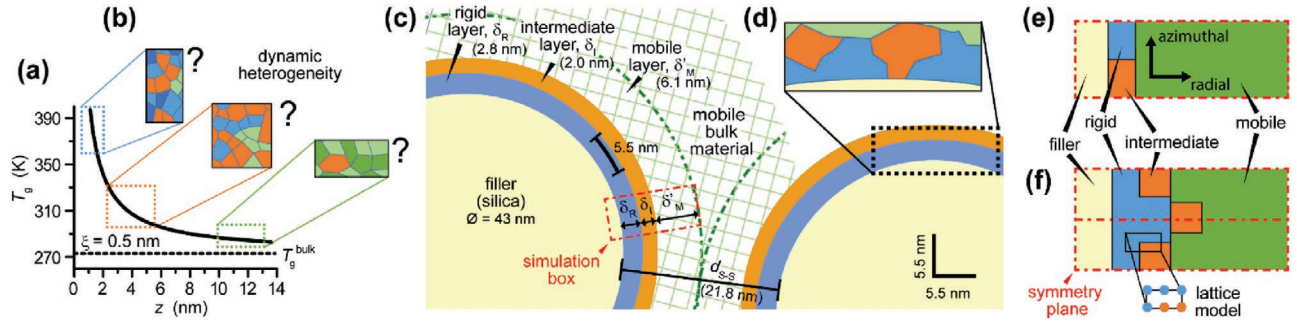

Figure 1. Mobility models for PNC. (a) T_g gradient in polymers close to an attractive surface as predicted by Equation (1) using $\xi = 0.5$ nm. (b) The spatial distribution of regions of dynamic heterogeneity, essentially characterized by low (blue), intermediate (orange), and high (green) bulk-like mobility, may vary along *z*. (c) Layer model of immobilized and intermediate-dynamics regions compared to (d) a scenario in which the filler surface is not entirely covered with fully immobilized material. Distances in (c) are to scale and belong to sample SiO_2-CG-PEA-1. (e) Lattice model in which the layer closest to the filler surface is characterized by both immobile and intermediate domains. (f) Representation of the models in (a–e) using a generic lattice model that mimics dynamic heterogeneity.

immobilized layer (also termed "interfacial layer")[21] in PNC is of the same numerical order as the dynamic heterogeneity length scale[20] and varies with the stiffness of the matrix polymer.[36] On the theory side, Simmons[37] has stressed the generality of the concept, which should apply to all dynamic interphases, for example, also those found in semicrystalline polymers and block copolymers with strong mobility contrast of the microphases.

The polymer matrix of a composite material is often subdivided into immobilized (also referred to as rigid/glassy/rigid-amorphous; *R*), intermediate (*I*) and mobile (*M*) regions to account for the experimental data in a minimal but sufficient model. Regions of intermediate mobility contribute to the mechanical reinforcement[4,25] and might result from two scenarios: i) the occurrence of an intermediate phase might be part of a 1D mobility gradient, in which a shell-like layer with in-between mobility is formed (Figure 1c), or, ii) the intermediate phase might be dominated by dynamic heterogeneity that is characteristic for polymers close to T_g, and hence for T_g gradients (Figure 1b). Due to heterogeneity at the filler surface, including incomplete binding of the polymer to the filler, the polymer layer next to the filler might contain both immobile and intermediate-dynamics material (Figure 1d). Structural implications are profound: in scenario (i), the intermediate phase would be a continuous shell-like layer that separates the immobilized phase from mobile bulk material, whereas in scenario (ii), the intermediate phase would be discontinuous, consisting of nanoscopic subdomains that are scattered between immobile and mobile sub-domains.

Recently, we have shown that bidirectional ^{1}H NMR spin diffusion (SD) experiments[38–41] are highly sensitive to how regions of different mobility are connected to each other.[42,43] In these experiments, magnetization transfer from rigid to mobile domains are compared to magnetization flow in the opposite direction, from mobile to rigid domains.[39] For phase-separated block-copolymers comprising mobile and a glassy polymer phase (PS-PB), the technique revealed asymmetric magnetization flow that could only be reproduced by considering intermixed immobile, intermediate, and mobile domains in the rigid-mobile transition area.[42] In a semicrystalline polyester (PCL), the intermediate phase did not form an in-between layer but formed nm-sized domains embedded in more rigid regions.[42] These findings provide direct support of Simmons' unified view of the relevance of dynamic heterogeneities in such materials.[37]

Here, we use bi-directional ^{1}H SD experiments to study the interphase in PNC for the first time. We focus on a set of so far unpublished results obtained several years ago for poly(ethyl acrylate) rubber filled with well-dispersed silica,[22,25] for which the T_g gradient model was proven to apply.[9] We extend our previous simulation model for SD data developed for layered systems[43] to accommodate the spatial requirements in PNC with spherical filler particles. The global fits to the whole data set do not allow for a clear preference of the shell versus the dynamic-heterogeneity model, but the relevant early stage of the SD process in our samples shows clear indications of the existence of lateral dynamic inhomogeneities in our samples.

2. Experimental Section

Experiments were performed on cross-linked poly(ethyl acrylate), PEA, that contains well-dispersed silicon oxide nanoparticles grafted with either 3-(trimethoxysilyl)propyl methacrylate, TPM, or *n*-octyltriethoxysilane, C8TES. The samples were identical to those of the previous studies.[22,25] TPM provided covalent bonding with the polymer matrix, whereas C8TES does not chemically bind to the polymer but just enhances filler-matrix compatibility and left only non-covalent bonds via hydrogen bonding to remaining surface-OH sites. The samples were referred to as SiO_2-CG-PEA-1 (filler particle diameter $d_{si} = 43$ nm; filler volume fraction $\phi_{si} = 0.22$) and SiO_2-CG-PEA-2 ($d_{si} = 27$; $\phi_{si} = 0.20$) for the covalently grafted (CG) TPM samples, and SiO_2-NCG-PEA ($d_{si} = 42$; $\phi_{si} = 0.29$) for the non-covalently grafted (NCG) C8TES sample.

Static ^{1}H NMR experiments were performed at 20 and 200 MHz proton resonance frequency (0.47 and 4.7 T magnetic field strength, respectively) using a Bruker minispec mq20 and a Bruker Avance III spectrometer, respectively. Except for the temperature-dependent measurements, the sample temperature was 80 °C, which is ≈100 K above the glass transition temperature of bulk PEA. The experiments exploit ^{1}H dipolar

© 2021 The Authors. Macromolecular Rapid Communications published by Wiley-VCH GmbH

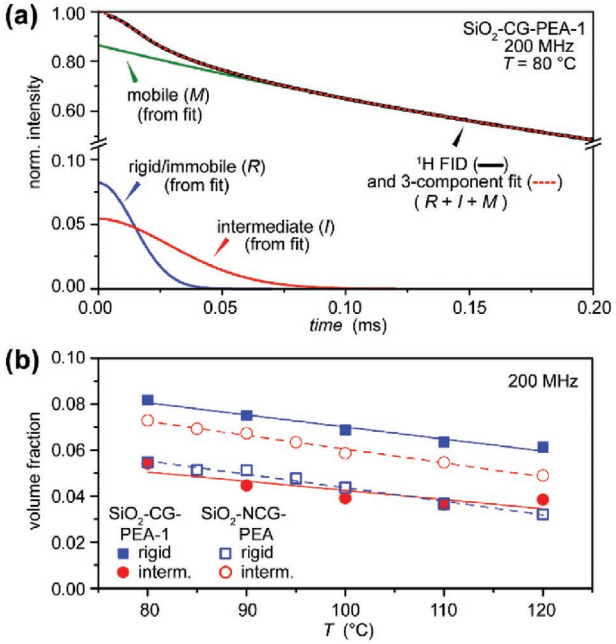

Figure 2. (a) Measured ^{1}H FID and decomposition of SiO_2-CG-PEA1 at T = 80 °C and 200 MHz. Colored lines are the individual components ($R/I/M$) from the fit, in this case not relying on magnetization filters (DQ, MAPE). (b) Temperature dependence of the rigid and intermediate phase in CG-A1 and NCG-A.

couplings that have a characteristic frequency of $\nu_{dip} \approx 20$ kHz. In this frequency range, the "NMR T_g" with a segmental relaxation time of $1/(2\pi \cdot 20\text{kHz}) \approx 10\,\mu\text{s}$ (rather than 100s) was about 273 K for PEA.[22] Well above and well below this temperature, the NMR response of bulk PEA was classified as mobile or rigid, respectively.

In the applied temperature range, the ^{1}H NMR free induction decay (FID) can be fitted using a minimal model comprising three components corresponding to the $R/I/M$ fractions of the polymer material;[39] see Figure 2a for representative data at 200 MHz. The unconstrained fit was possible because of the rather short receiver dead time (4 µs) and the good signal-to-noise ratio. The results were in qualitative agreement with previous results obtained for the same samples several years before,[22] only the phase fractions were somewhat smaller, possibly indicating aging effects. This was why it was chosen to focus on SD experimental data obtained at low field already in the context of the earlier study, which was not published yet. The used temperature of 80 °C represented a compromise of having sufficient signal from the dynamically more restricted components, and at the same time being able to separate it reliably from the mobile matrix with long T_2.

For low-field measurements, FID detection was additionally preceded by a pulsed magic-sandwich echo (MSE) to bridge the long dead time of 15 µs.[39,44] The time-domain NMR SD experiments utilized a selective excitation of either the mobile or the most immobile phase by magic-and-polarization echo (MAPE or MP in indices) or double-quantum (DQ) filters, respectively, followed by a magnetization mixing period (t_{mix}) and subsequent NMR signal detection to reveal the flux of magnetization from one mobility domain to another. The filters were set such that the intermediate-phase signal was practically absent in the filtered signals. Pulse sequences and data treatment for FID decomposition were presented in previous works[39–41,44] and will not be discussed here.

In the present context, several hundred ^{1}H spins contribute to SD even if local domains were addressed, and SD follows Fick's law of diffusion. The partial differential equation was solved on a 1D, 2D, or 3D simulation grid that mimics the characteristic sample morphology. For the same volume fractions and similar alignment of the nanoscopic $R/I/M$ domains, straight-line phase boundaries resulted in virtually the same SD behavior as irregular, more realistic phase boundaries.[42] The generic model in Figure 1f can thus be understood as a minimal but sufficient representation of more complex morphologies. Details on the simulation protocol and associated equations are presented in ref. [43].

3. Results and Discussion

The filler particles are mostly homogeneously distributed in our samples with an average surface-to-surface distance, $d_{S\text{-}S}$, of about 22 and 15 nm (see **Table 1** and the Supporting Information). Thus, particle-particle contacts are rare, as proven by a linear correlation of the rigid and intermediate phase fractions with the silica content.[22] Clustering affects the apparent NMR domain sizes[45] and hence the fitted SD coefficient (SDC). In this study, we do not apply SD experiments to determine domain sizes but elucidate the extent of dynamic heterogeneity in particle-filled rubber by exploring how immobile, intermediate, and mobile domains are distributed inside the rigid-mobile mobility gradient region. Deviations from the

Table 1. Volume fractions (ϕ) measured at 20 MHz and characteristic length distances (δ, d) for the PEA samples[22] at 80 °C where the indices SiO_2 and $R/I/M$ indicate silica particles and the most immobile ("rigid"), intermediate, and mobile phase of the polymer matrix, respectively. $d_{S\text{-}S}$ equals the average surface-to-surface distance between the filler particles that was benchmarked relative to a body-centered cubic lattice of filler particles. ϕ'_M and δ'_M characterize that part of the mobile phase that surrounds the filler particle; see text. Polymer fractions are normalized to $\phi_R + \phi_I + \phi_M = 1$. For absolute volume fractions, the polymer volume fractions have to be multiplied by $(1-\phi_{SiO_2})$. Uncertainties in ϕ are about ±0.03. Layer size uncertainties are ±0.1 nm. d_{SiO_2} are mean values of a narrow size distribution (width of less than 20% of the average diameter).

Sample	ϕ_{SiO_2}	d_{SiO_2} [nm]	$d_{S\text{-}S}$ [nm]	ϕ_R	ϕ_I	ϕ_M	ϕ'_M	δ_R [nm]	δ_I [nm]	δ'_M [nm]
SiO_2-CG-PEA-1	0.216	43	21.8	0.121	0.106	0.773	0.441	2.8	2.0	6.1
SiO_2-CG-PEA-2	0.202	27	14.6	0.210	0.179	0.611	0.285	2.6	2.3	2.4
SiO_2-NCG-PEA	0.293	42	15.2	0.100	0.080	0.820	0.452	1.3	1.4	4.9

© 2021 The Authors. Macromolecular Rapid Communications published by Wiley-VCH GmbH

idealized spatial extension of each phase will affect the absolute values of the fitted SDC, but not the conclusions regarding the suitability of the underlying morphology model in reproducing the experimental data.

Evaluating the equilibrium NMR signal intensity without magnetization filtering (Figure 2a), we find that the most immobilized regions (*R*) have an overall similar volume fraction as the intermediate regions (Table 1). The volume fraction of the immobilized phase exceeds that of the intermediate phase by a mere 15–25% (uncertainty $u(\phi) = \pm 0.03$). Associated domain sizes ($\delta_R, \delta_I, \delta'_M$) can be calculated from the NMR volume fractions (ϕ_M, ϕ_I, ϕ_R; see the Supporting Information), assuming well-separated shell-like layers for the moment. In this model, the layer size of the mobile phase corresponds to half the distance between intermediate layers, $\delta'_M = d_{S\text{-}S}/2 - (\delta_R + \delta_I)$, and represents not all of the mobile bulk material ($\phi'_m < \phi_m$) but just that part that forms a shell-like layer around the filler particle; see again Figure 1c and Table 1.

The total reduced-mobility layer size (comprising most immobilized and intermediate components) in CG-PEA is 4.8–4.9 nm (2.6–2.8 nm for the rigid phase). For NCG-PEA, the size of the rigid phase is just 1.3 nm, but the combined immobilized and intermediate layers have a thickness of 2.7 nm. The reduced-mobility fractions in CG and NCG PEA samples show essentially the same temperature (*T*) dependence (the same slope with *T*; see Figure 2b), suggesting a similar organization of the mobility gradient in CG and NCG samples. Note that protons from the covalently bonded grafter molecules represent a significant fraction of the most rigid component at the highest temperatures.[9,22] This means that the latter fraction is not just composed of pure PEA polymer but chemically mixed. Upon increasing the temperature from 80 to 120 °C, the volume fraction of the reduced-mobility layer decreases by about 26 and 37% for CG PEA, and NCG PEA, respectively. Adhesion and binding to the filler surface are not expected to show noticeable temperature effects over the studied temperature range (350–390 K): the energy gain associated with hydrogen bonding is comparable to, or larger than, 2 k_BT (5 kJ mol^{-1}, or 600 K equivalent temperature),[46,47] and is even larger for covalent binding. Nevertheless, CG PEA shows a larger immobilized polymer fraction than NCG PEA. As a consequence of physical adhesion, a polymer chain close to the filler surface is likely to adhere to the filler surface at multiple places, reducing the opportunity for other polymer chains to bind to the filler. For CG samples with high or intermediate grafter densities (1.5–3.2 nm^{-2} in our samples),[22] assuming one grafter molecule binds one polymer chain, this leads to excess binding at CG surfaces relative to mere physical adhesion (NCG samples). This, in turn, will increase the amount of immobilized material, yet with a similar temperature dependence of the mobility gradient as for physical adhesion, in agreement with the experimental data. Heterogeneous binding at the filler surface will additionally promote dynamic heterogeneity in this region.

To learn about the spatial alignment of the nanoscopic rigid, intermediate, and mobile domains in PEA, we next conducted bidirectional ^{1}H SD experiments, that is, exploiting rigid-to-mobile (DQ filter) versus mobile-to-rigid (MAPE filter) magnetization transfer. All PEA samples show asymmetric buildup curves in that the signal of the intermediate phase rises either before (**Figure 3**a,c–e, DQ-filtered curves), or virtually simultaneously with (Figure 3b,f–h, MAPE-filtered curves), the signal of the second sink phase. This behavior is reminiscent of our earlier data on the phase-separated block-copolymer PS-*b*-PB, the experimental data of which could not be reproduced using a simple shell-like layer.[42,43] Instead, intermixed *R*/*I*/*M* phases inside the rigid-mobile transition region were required to mimic the experimental data. However, in the case of thin intermediate layers and fast SD in the rigid and intermediate phases, magnetization originating from the mobile phase can quickly cross the intermediate layer ($t^*_{mix} = d_i^2/2D_i \sim$ 1–4 ms; note the $t^{1/2}_{mix}$-axes in Figure 3), and clear detection of the expected delayed rise of the rigid-phase signal is difficult given the limited accuracy of the data. Studying magnetization flow in the opposite direction (out of the rigid phase) does not provide a qualitative distinction, as SD into the mobile phase is anyways slower as SD into the intermediate phase.

To clarify whether the data can be adequately reproduced by shell-like layers, or if intermixed *R*/*I*/*M* domains are required, and to eventually conclude on possible dynamical similarities between the rigid and intermediate phase, we performed SD simulations using variations of the generic model in Figure 1f. Shell-like layers can most easily be described in a 1D layer model using the distances specified in Table 1, that is, stacked rigid, intermediate, and mobile domains (cf. simulation box in Figure 1c). Dynamically heterogeneous scenarios, on the other hand, require 2D or 3D modeling (Figure 1e,f). Each of these 1D, 2D, or 3D models represents a fraction of the polymer material in the radial direction from the center of the filler particle. Any curvature of the shell-like layers was ignored: after 50 ms SD mixing (the period after which the buildup curves show their maximum), assuming an average SDC of 0.3 nm² ms^{-1}, the 1D mean-square displacement is ≈5.5 nm, which is small compared to the curvature radius of the filler particles and the immobilized polymer layer (cf. Figure 1c). There is no SD across the silica filler particle due to its lack of ^{1}H spins, which was accounted for in the simulations by assuming a (thin) filler layer with vanishing SD efficiency. For each of the 1D/2D/3D morphology variants, we then optimized the NMR SD parameters (SDC's: $D_M < D_I \leq D_R$; spin-lattice relaxation times: $T_{1M} < T_{1I} \leq T_{1R}$) until best agreement with the experimental DQ- and MAPE-filtered data sets was achieved by minimizing

$$\Delta_{DQ,MP} = \sqrt{(\Delta_M^2 + \Delta_I^2 + \Delta_R^2)/3}, \text{ where} \quad (2)$$

$$\Delta_k = \sqrt{\sum_N^{j=1} \frac{1}{N} (f_{k,j}^{exp} - f_{k,j}^{sim})^2} \quad (3)$$

Here, f_k^{exp} and f_k^{sim} are the experimental and simulated data of each phase ($k = R/I/M$), normalized such that the maximum of all f_k^{exp} and f_k^{sim} (the initial value of the source curve) equals 1. In doing so we consider that the absolute variations, caused by experimental and fitting ambiguities, are of the same order of magnitude for the sink- and the source curves. The deviations were separately calculated for MAPE- and DQ-filtered curves but were fit simultaneously using one and the same sample morphology and SD parameters. We compared best-fit

© 2021 The Authors. Macromolecular Rapid Communications published by Wiley-VCH GmbH

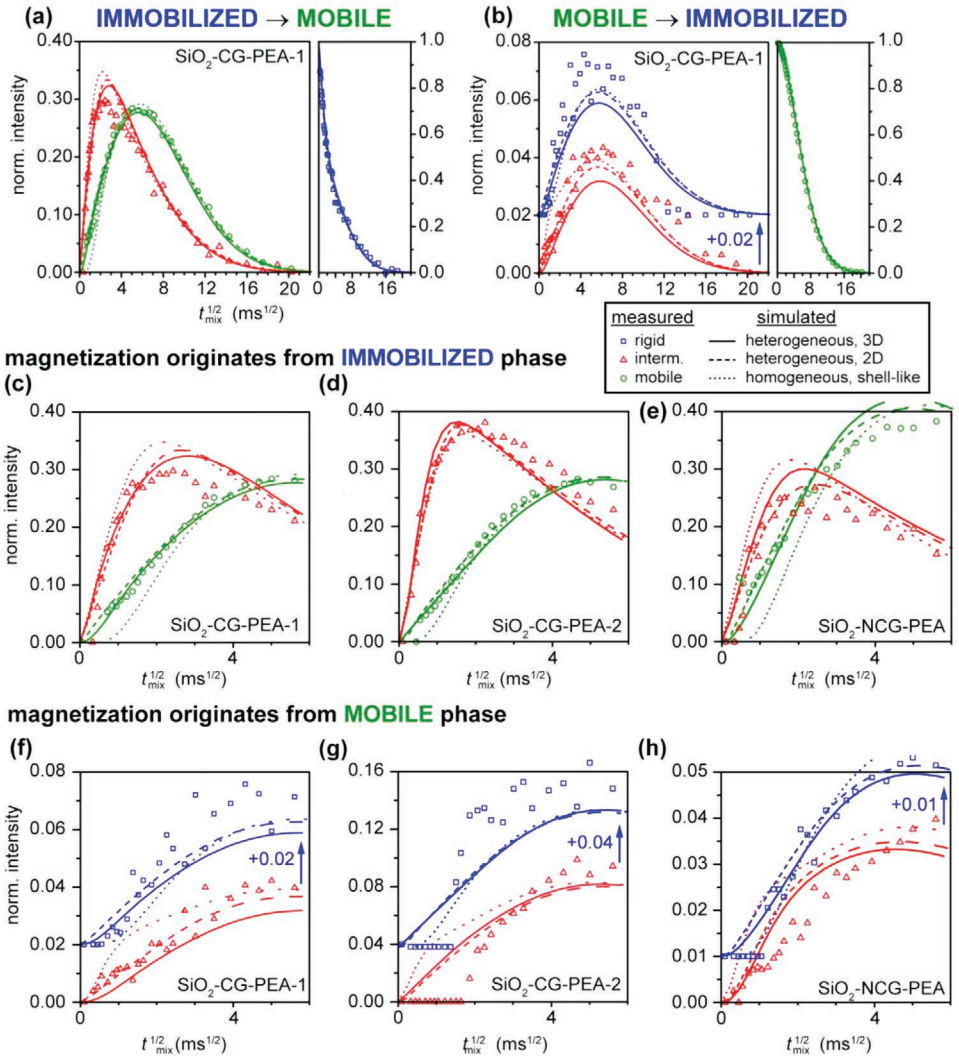

Figure 3. Bidirectional SD curves: (a,b) Measured data sets for sample SiO_2-CG-PEA-1 (immobilized/rigid phase: blue squares; intermediate phase: red triangles; mobile phase: green circles) and associated simulated SD curves (see text and Figure 4 for model descriptions) that were simultaneously fitted to the rigid-phase and mobile-phase filtered data. Lower panels: Close-ups of data for all three samples for immobilized to mobile (c–e) and mobile to immobilized polarization transfer (f–h). For clarity in the latter, simulated curves of the rigid phase and the associated experimental data were vertically shifted.

results from shell-like layers to those from 2D and 3D models (**Figure 4**), for which we focused on two scenarios: i) deviations from a simple layer model resulting from a dynamically heterogeneous coverage of the filler particle with rigid and intermediate polymer segments (Figure 4b), including direct contact between the rigid and mobile phase, and, ii) intermixed *R*/*I*/*M* domains that avoid *R*–*M* direct contacts, resembling a more balanced but still dynamically heterogeneous mobility gradient (Figure 4c). Along the lines of our previous work,[42,43] the latter models were parameterized with a minimal set of up to 3 parameters each, for which a manual grid search was performed, coupled with a final numerical optimization of all parameters. We note that a phase boundary between the rigid and mobile phase is a simplified representation of a steep mobility gradient and should not be overvalued in physical or morphological terms.

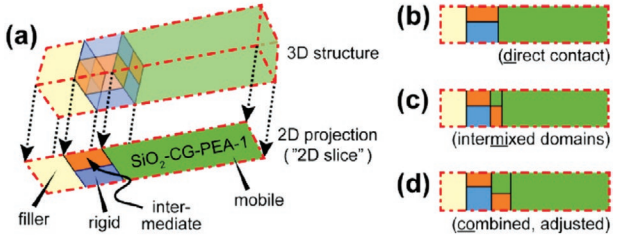

Figure 4. Morphology models as used in the SD simulations, exemplified using the volume fractions in SiO_2-CG-PEA-1. (a) 3D model and associated 2D projection. (b–d) 2D models for the case of (b) direct contact, (c) intermixed rigid, intermediate, and mobile domains, and d) an optimized model that combines aspects from models (b) and (c).

The best 1D, 2D, and 3D SD simulations match the experimental data equally well: the fitting accuracy increases only marginally upon accounting for dynamical heterogeneity in

© 2021 The Authors. Macromolecular Rapid Communications published by Wiley-VCH GmbH

Table 2. SD parameters (D_k, T_{1k}, k = {R,I,M}) and fitting accuracies $\left(\Delta_{DQ}, \Delta_{MP}, \overline{\Delta} = \sqrt{(\Delta_{DQ}^2 + \Delta_{MP}^2)/2}\right)$ of the PEA samples for intermixed (*mi*) $R/I/M$ domains, a steep mobility gradient as represented by direct (*di*) contact between the R/I and M domains, and a combined (*co*) model containing aspects of the former two (Figure 4), compared to the results of a simple shell-like model (*shell*). Subscripts "DQ" and "MP" refer to rigid-phase- and mobile-phase-filtered SD experiments, respectively. The size of the simulation box is reported in the form of $r \times a \times b$, where r denotes the radial distance from the center of the filler particle, and $a = b$ are azimuthal dimensions perpendicular to r. SDC's have a systematic uncertainty of less than ≈10% (see the Supporting Information), where values larger than 0.8 nm² ms^{-1} were not accounted for in the reported averages.

Sample	type	dim.	size [nm^{dim}]	D_R	D_I [nm² ms^{-1}]	D_M	T_{1R}	T_{1I} [ms]	T_{1M}	Δ_{DQ}	Δ_{MP}	$\overline{\Delta}$
SiO_2-CG-PEA-1	mi	3	22 × 6 × 6	0.30	0.30	0.07	220	130	58	1.56	0.59	1.18
		2	22 × 6	0.35	0.35	0.07	220	130	58	1.49	0.57	1.13
	di	3	22 × 6 × 6	0.50	0.06	0.06	300	70	60	1.62	0.90	1.31
		2	22 × 6	0.50	0.25	0.06	300	100	60	1.32	0.81	1.10
	co	3	22 × 6 × 6	0.30	0.30	0.06	220	130	58	1.47	0.63	1.13
		2	22 × 6	0.35	0.35	0.06	220	130	58	1.28	0.60	1.00
	shell	1	22	0.40	0.40	0.07	195	120	61	1.64	0.87	1.31
SiO_2-CG-PEA-2	mi	3	15 × 4 × 4	0.8	0.8	0.08	100	100	65	2.43	1.32	1.96
		2	15 × 4	(1.00)	(1.00)	0.09	100	100	65	2.34	1.22	1.87
	di	3	15 × 4 × 4	0.30	0.30	0.12	90	90	65	2.47	1.26	1.96
		2	15 × 4	0.50	0.50	0.10	100	100	65	2.22	1.20	1.78
	shell	1	15	(1.00)	(1.00)	0.095	100	100	64	2.48	1.31	1.98
SiO_2-NCG-PEA	mi	3	15 × 4 × 4	0.20	0.15	0.04	250	150	55	2.59	0.54	1.87
		2	15 × 4	0.20	0.20	0.04	250	250	55	2.48	0.44	1.78
	di	3	15 × 4 × 4	0.12	0.12	0.06	400	400	60	2.60	0.67	1.90
		2	15 × 4	0.20	0.15	0.05	400	300	60	2.33	0.67	1.71
	shell	1	15	0.15	0.15	0.05	350	100	58	2.63	0.46	1.89
all PEA samples, average				0.3 ± 0.17	0.2 ± 0.17	0.0 ± 0.02	2 4 ± 100	1 7 ± 85	6 ± 3			

the rigid-mobile transition area (Figure 3; Δ values in **Table 2**). Based upon this argument alone, the overall SD time evolution does not allow for a unique conclusion on the applicability of the shell versus the 3D-dynamic-inhomogeneity model, irrespective of covalent or non-covalent grafting.

Our best-fit SDC's are affected by the underlying morphology model (Table 2). The suitability of each model can be cross-validated by considering that SD in rigid and semi-flexible domains adopts values in the range of 0.2–0.8 nm² ms^{-1}, while mobile regions commonly show SD efficiencies of less than 0.1 nm² ms^{-1}.[38,40,41,43,45,48] We find average values of D_R = (0.35 ± 0.17) nm² ms^{-1}, D_I = (0.29 ± 0.17) nm² ms^{-1}, and D_M = (0.07 ± 0.02) nm² ms^{-1}, excluding outliers with D_k > 0.8 nm² ms^{-1} (bracketed in Table 2; a maximum value of 1.0 was enforced in our calculations). The fitted SDC of the intermediate phase tends to be close to the SD efficiency in the rigid phase, though good fits with $D_I \approx D_M$ are possible (data not shown). This trend indicates that segmental flexibility in intermediate domains is close (but not identical) to that in immobile domains.

For SiO_2-CG-PEA-2, the shell-like model and intermixed $R/I/M$ domains both require surprisingly high SDC's outside the anticipated range of 0.2–0.8 nm² ms^{-1}.[38,40,41,43,45,48] 2D and 3D models that allow for direct contact between the rigid and mobile domains (Figure 4b) overcome this shortcoming, suggesting dynamic heterogeneity in the vicinity of the filler particle. As noted in the introductory part, this insight does not contradict the concept of an overall smooth mobility gradient. Instead, a model that combines features from Figure 4b,c might be best suited. To test this hypothesis, we turned back to sample SiO_2-CG-PEA-1 and tried if such a model would also perform best on this sample (Figure 4d). Despite only modest improvements, the then optimized model yields Δ values that are in line with the hypothesis.

We finally varied the size of the simulation box in azimuthal direction (and hence the length scale of heterogeneities) to exclude bias effects from this parameter. Increasing the lateral dimension from $a = b$ = 4 nm to a = b = 30 nm increases the best-fit SDC of the rigid and intermediate phase by a mere 7%, with no significant changes in fitting accuracy. Bias effects arising from the azimuthal size of the simulation box can thus be excluded. Low sensitivity to the azimuthal size of the rigid and intermediate domains agrees with the fact that 1D layer simulations, which are not affected by the azimuthal size of the simulation box, can reproduce the experimental data reasonably well.

With all aspects considered, the best direct piece of evidence for the relevance of dynamic heterogeneities is thus the early-stage build-up of intermediate-phase signal in the mobile-phase-filtered SD experiments highlighted in Figure 3f–h, which occurs as quickly as the signal of the rigid-phase rises. As it is obvious from these close-ups, any shell-based model

© 2021 The Authors. Macromolecular Rapid Communications published by Wiley-VCH GmbH

intrinsically predicts a quicker initial rise of the intermediate as compared with the rigid phase signal. This is not observed, but the limited accuracy of the data makes a definite conclusion difficult. Clearly though, the "heterogeneous" models capture the initial rise notably better, however at the expense of an inferior fit at longer times. The latter can be ascribed to the simplicity of the used models and is strongly affected by longitudinal relaxation, the complexities of which, such as T_1 gradients coupled to mobility gradients, cannot be captured with our model.

4. Conclusions

In summary, our bidirectional NMR SD data on silica-filled PEA rubber samples with covalent as well as non-covalent surface grafting reveal that the spatial distribution of material with reduced mobility is overall well represented by both, a model assuming a shell-like layer of immobilized and intermediate-dynamics material, and by models assuming a lateral arrangement of nanometer-sized dynamic heterogeneities. The fitted SD coefficients strongly suggest that the intermediate phase as characterized by NMR is subjected to reduced segmental flexibility that resembles that in the rigid phase. Only the better fits in the early stages of SD provide indications towards the relevance of dynamic heterogeneities, which could more clearly be confirmed for the interphase in PS-PB block-copolymers and in a semicrystalline polyester.[43] Early-stage SD is more sensitive to the detailed sample morphology than later-stage SD, noting that the former contains information on potential time lags needed to spatially cross one region before reaching another, while late-stage spin-diffusion is increasingly dominated by (spatially less sensitive) T_1-relaxation. The limitations in overall accuracy are mostly related to the rather low relative intensity of the sink phases in the mobile-phase-filtered SD experiments. Current and future work is thus directed at investigating PNCs with higher filler loading and larger fractions of mobility-reduced material, as well as performing analogous experiments at higher magnetic field strength. This also provides longer T_1 relaxation times, thus addressing also the related shortcoming of increased fitting interdependencies and the decreased distinction between different models at low field. An important open question is also the role of surface roughness of the silica particles, which has so far hardly been addressed in experimental works.

Supporting Information

Supporting Information is available from the Wiley Online Library or from the author.

Acknowledgements

The authors acknowledge funding by the Deutsche Forschungsgemeinschaft (DFG, German Research Foundation), project-IDs 316439043 (SA982/13-1) and 189853844 (SFB-TRR 102), and a postdoctoral fellowship by the German National Academy of Sciences (grant number LPDS-2017-14 to M.R).

Open access funding enabled and organized by Projekt DEAL.

Conflict of Interest

The authors declare no conflict of interest.

Data Availability Statement

Research data are not shared.

Keywords

confinement, filled elastomers, interphase, nanocomposites, NMR spin diffusion, T_g gradient

Received: January 27, 2021
Revised: February 26, 2021
Published online: March 24, 2021

[1] M. J. Wang, *Rubber Chem. Technol.* **1998**, *71*, 520.
[2] A. H. El-Hag, L. C. Simon, S. H. Jayaram, E. A. Cherney, *IEEE Trans. Dielectr. Electr. Insul.* **2006**, *13*, 122.
[3] M. J. Wang, *Rubber Chem. Technol.* **1999**, *72*, 430.
[4] A. Mujtaba, M. Keller, S. Ilisch, H. J. Radusch, M. Beiner, T. Thurn-Albrecht, K. Saalwächter, *ACS Macro Lett.* **2014**, *3*, 481.
[5] A. A. Gusev, *Macromolecules* **2006**, *39*, 5960.
[6] D. Long, P. Sotta, *Rheol. Acta* **2007**, *46*, 1029.
[7] S. Merabia, P. Sotta, D. R. Long, *Macromolecules* **2008**, *41*, 8252.
[8] P. Klonos, A. Kyritsis, P. Pissis, *Polymer* **2016**, *84*, 38.
[9] A. Papon, H. Montes, M. Hanafi, F. Lequeux, L. Guy, K. Saalwächter, *Phys. Rev. Lett.* **2012**, *108*, 065702.
[10] S. E. Harton, S. K. Kumar, H. Yang, T. Koga, K. Hicks, H. Lee, J. Mijovic, M. Liu, R. S. Vallery, D. W. Gidley, *Macromolecules* **2010**, *43*, 3415.
[11] N. Suzuki, M. Ito, F. Yatsuyanagi, *Polymer* **2005**, *46*, 193.
[12] T. Glomann, G. J. Schneider, J. Allgaier, A. Radulescu, W. Lohstroh, B. Farago, D. Richter, *Phys. Rev. Lett.* **2013**, *110*, 178001.
[13] T. Glomann, A. Hamm, J. Allgaier, E. G. Hübner, A. Radulescu, B. Faragoc, G. J. Schneider, *Soft Matter* **2013**, *9*, 10559.
[14] M. Krutyeva, A. Wischnewski, M. Monkenbusch, L. Willner, J. Maiz, C. Mijangos, A. Arbe, J. Colmenero, A. Radulescu, O. Holderer, M. Ohl, D. Richter, *Phys. Rev. Lett.* **2013**, *110*, 108303.
[15] K. U. Kirst, F. Kremer, V. M. Litvinov, *Macromolecules* **1993**, *26*, 975.
[16] A. Kusmin, S. Gruener, A. Henschel, N. de Souza, J. Allgaier, D. Richter, P. Huber, *Macromolecules* **2010**, *43*, 8162.
[17] S. Y. Kim, H. W. Meyer, K. Saalwächter, C. F. Zukoski, *Macromolecules* **2012**, *45*, 4225.
[18] J. P. Cohen-Addad, C. Roby, M. Sauviat, *Polymer* **1985**, *26*, 1231.
[19] N. Jouault, D. Zhao, S. K. Kumar, *Macromolecules* **2014**, *47*, 5246.
[20] C. Cheng, A. P. Sokolov, *J. Chem. Phys.* **2020**, *152*, 094904.
[21] I. Popov, B. Carroll, V. Bocharova, A. C. Genix, S. Cheng, A. Khamzin, A. Kisliuk, A. P. Sokolov, *Macromolecules* **2020**, *53*, 4126.
[22] A. Papon, K. Saalwächter, K. Schaler, L. Guy, F. Lequeux, H. Montes, *Macromolecules* **2011**, *44*, 913.
[23] J. Berriot, F. Lequeux, L. Monnerie, H. Montes, D. Long, P. Sotta, *J. Non-Cryst. Solids* **2002**, *307*, 719.
[24] A. Sargsyan, A. Tonoyan, S. Davtyan, C. Schick, *Eur. Polym. J.* **2007**, *43*, 3113.
[25] A. Papon, H. Montes, F. Lequeux, J. Oberdisse, K. Saalwächter, L. Guy, *Soft Matter* **2012**, *8*, 4090.
[26] S. Napolitano, E. Glynos, N. B. Tito, *Rep. Prog. Phys.* **2017**, *80*, 036602.

© 2021 The Authors. Macromolecular Rapid Communications published by Wiley-VCH GmbH

[27] J. L. Keddie, R. A. L. Jones, R. A. Cory, *Europhys. Lett.* **1994**, *27*, 59.
[28] J. Berriot, H. Montes, F. Lequeux, D. Long, P. Sotta, *Macromolecules* **2002**, *35*, 9756.
[29] J. L. Keddie, R. A. L. Jones, R. A. Cory, *Faraday Discuss.* **1994**, *98*, 219.
[30] J. Q. Pham, P. F. Green, *J. Chem. Phys.* **2002**, *116*, 5801.
[31] D. Long, F. Lequeux, *Eur. Phys. J. E: Soft Matter Biol. Phys.* **2001**, *4*, 371.
[32] S. Merabia, P. Sotta, D. Long, *Eur. Phys. J. E: Soft Matter Biol. Phys.* **2004**, *15*, 189.
[33] A. Dequidt, D. R. Long, P. Sotta, O. Sanseau, *Eur. Phys. J. E: Soft Matter Biol. Phys.* **2012**, *35*, 61.
[34] U. Tracht, M. Wilhelm, A. Heuer, H. Feng, K. Schmidt-Rohr, H. W. Spiess, *Phys. Rev. Lett.* **1998**, *81*, 2727.
[35] S. Merabia, D. Long, *Eur. Phys. J. E: Soft Matter Biol. Phys.* **2002**, *9*, 195.
[36] S. Cheng, B. Carroll, W. Lu, F. Fan, J. M. Y. Carrillo, H. Martin, A. P. Holt, N. G. Kang, V. Bocharova, J. W. Mays, B. G. Sumpter, M. Dadmun, A. P. Sokolov, *Macromolecules* **2017**, *50*, 2397.
[37] D. S. Simmons, *Macromol. Chem. Phys.* **2016**, *217*, 137.
[38] J. Clauss, K. Schmidt-Rohr, H. W. Spiess, *Acta Polym.* **1993**, *44*, 1.
[39] M. Mauri, Y. Thomann, H. Schneider, K. Saalwachter, *Solid State Nucl. Magn. Reson.* **2008**, *34*, 125.
[40] H. W. Meyer, H. Schneider, K. Saalwächter, *Polym. J.* **2012**, *44*, 748.
[41] K. Schäler, M. Roos, P. Micke, Y. Golitsyn, A. Seidlitz, T. Thurn-Albrecht, H. Schneider, G. Hempel, K. Saalwächter, *Solid State Nucl. Magn. Reson.* **2015**, *72*, 50.
[42] M. Roos, K. Schäler, A. Seidlitz, T. Thurn-Albrecht, K. Saalwächter, *Colloid Polym. Sci.* **2014**, *292*, 1825.
[43] H. Schneider, K. Saalwächter, M. Roos, *Macromolecules* **2017**, *50*, 8598.
[44] A. Maus, C. Hertlein, K. Saalwächter, *Macromol. Chem. Phys.* **2006**,*207*, 1150.
[45] E. G. Sorte, A. L. Frischknecht, T. M. Alam, *Phys. Rev. Mater.* **2019**, *3*, 204819.
[46] O. Markovitch, N. Agmon, *J. Phys. Chem. A* **2007**, *111*, 2253.
[47] D. van der Spoel, P. J. van Maaren, P. Larsson, N. Timneanu, *J. Phys. Chem. B* **2006**, *110*, 4393.
[48] E. G. Sorte, L. J. Abbott, A. L. Frischknecht, M. A. Wilson, T. M. Alam, *J. Polym. Sci., Part B: Polym. Phys.* **2018**, *56*, 62.

© 2021 The Authors. Macromolecular Rapid Communications published by Wiley-VCH GmbH